PHYSICAL REVIEW B **78**, 054428 (2008)

Impurity-ion pair induced high-temperature ferromagnetism in Co-doped ZnO

C. D. Pemmaraju,[1] R. Hanafin,[1] T. Archer,[1] H. B. Braun,[2] and S. Sanvito[1]
[1]*School of Physics and CRANN, Trinity College, Dublin 2, Ireland*
[2]*School of Physics, University College Dublin, Dublin 4, Ireland*
(Received 8 April 2008; revised manuscript received 24 June 2008; published 19 August 2008)

Magnetic 3*d* ions doped into wide-gap oxides show signatures of room-temperature ferromagnetism, although their concentration is two orders of magnitude smaller than that in conventional magnets. The prototype of these exceptional materials is Co-doped ZnO, for which an explanation of the room-temperature ferromagnetism is still elusive. Here we demonstrate that magnetism originates from Co^{2+} oxygen-vacancy pairs with a partially filled level close to the ZnO conduction-band minimum. The magnetic interaction between these pairs is sufficiently long ranged to cause percolation at moderate concentrations. However, magnetically correlated clusters large enough to show hysteresis at room temperature already form below the percolation threshold and explain the current experimental findings. Our work demonstrates that the magnetism in ZnO:Co is entirely governed by intrinsic defects and a phase diagram is presented. This suggests a recipe for tailoring the magnetic properties of spintronics materials by controlling their intrinsic defects.

DOI: 10.1103/PhysRevB.78.054428 PACS number(s): 75.50.Pp, 71.20.−b, 71.55.−i

I. INTRODUCTION

ZnO is a piezoelectric conductive oxide in which free carriers coexist with optical transparency.[1,2] If made magnetic, ZnO will become the ultimate multifunctional material with semiconducting, magnetic, optical, and mechanical properties. This will have a far reaching impact on the emerging field of spintronics[3] with applications in optoelectronics[4] and quantum computing.[5] Moreover it will allow us to go beyond the (Ga,Mn)As paradigm[6] whose practical use is severely hampered by the low ferromagnetic critical temperature. This is why ZnO:Co is perhaps the most studied among all the diluted magnetic oxides. Room-temperature ferromagnetism (RTF), first demonstrated by Ueda *et al.*,[7] is now confirmed by a number of groups.[8–10] The experimental situation is however still confused and populated by somehow contradictory results. Here we list the main findings.

(i) Spectroscopy confirms that Co^{2+} substituting Zn is the center responsible for all the different magnetic phases found experimentally, including RTF,[11–13] paramagnetism,[12,14] and spin glasses.[15] RTF is usually assigned from magnetometry.[7–10]

(ii) The saturation magnetization M_s and the remanence are always small and secondary phases are often difficult to rule out. However, except for metallic Co, most of them are either nonmagnetic or antiferromagnetic with low Néel temperatures (CoO, Co_2O_3, Co_3O_4, and $ZnCo_2O_4$). The coercive field is typically small ($\sim$100 Oe) and only weakly temperature dependent.

(iii) M_s is usually smaller than what is expected for Co^{2+} with values as low as 0.01 μ_B/Co,[12] suggesting antiferromagnetic interaction among Co^{2+} and frustration.[13,14,16,17]

(iv) Growth conditions and annealing are crucial for the magnetic state. Chemical methods[14,16] and molecular-beam epitaxy[18] generally lead to paramagnetism, while pulsed laser deposition produces RTF films.[7–10] Typically oxygen deficient growth[10] at tuned substrate temperatures[19–21] promotes RTF. Similarly, annealing in vacuum enhances the magnetic moment and produces ferromagnetism,[12,21–23] while annealing in oxygen has the opposite effect.[23,24] Clearly sample morphology and intrinsic defects are important for the magnetic state.

(v) The role played by free carriers in establishing magnetism is unclear. Sequential annealing in reducing and oxidizing atmosphere reveals little correlation between the electrical conductivity and the magnetic state.[25] Similar conclusions are reached for Al and H doping.[26] In general ferromagnetism is found in both insulating and metallic films[27] although samples with similar carrier and Co densities can also be found paramagnetic.[28]

(vi) ZnO is often reported to be oxygen deficient. This has been attributed to either oxygen vacancies (V_O) (Refs. 29 and 30) or interstitial H,[31] with Zn interstitials (Zn_i) now ruled out by both experimental[29] and theoretical[30,31] evidences. Thus the promotion of RTF due to Zn vapor exposure[32,33] can be hardly attributed to an increase of the Zn_i concentration, and may be reinterpreted as originating from an increase of the V_O concentration.

(vii) Electron paramagnetic resonance[34] suggests the presence of two magnetic centers. These are both related to Co^{2+}, although they exhibit fine differences in the signal. Interestingly, for a nominal Co concentration about 5% the two centers appear with similar abundance. Very recent studies based on Raman spectroscopy,[35] x-ray absorption near-edge structure spectroscopy,[36] and resonant inelastic x-ray scattering[37] have attributed such second center to the presence of oxygen vacancies.

In this work we investigate theoretically the ferromagnetism of ZnO:Co by using a combination of state of the art density-functional theory electronic structure method and Monte Carlo simulations for effective Hamiltonian. We will demonstrate that the ferromagnetism originates from a subtle interplay between strong near range magnetic interaction between Co^{2+} ions substitutive to Zn and a long-range coupling between Co^{2+} oxygen vacancy pairs. Based on our calculations we propose a phase diagram for ZnO:Co that is put to the test of the existing experimental data.

II. DISCUSSION OF EXISTING MECHANISMS FOR FERROMAGNETISM

Existing mechanisms for ferromagnetism in the diluted limit cannot explain this complex collection of phenomena. The *p-d* Zener model[38] lacks of its foundations when applied to $Zn_{1-x}Co_xO$ since it is difficult to establish a clear correlation between carriers and magnetism.[25–28] When present, carriers are electrons and not holes with small exchange coupling to the local spins and therefore the typical critical temperatures (T_C) are tiny at realistic carrier densities. Similarly superexchange must be ruled out.[39] This is short ranged and RTF can be obtained only for x above the nearest-neighbor (NN) percolation threshold. For the wurtzite lattice this is 20%, much greater than the typical experimental concentrations.

Rather often a modification of the Zener scheme, called the donor impurity band exchange[40] (DIBE), is claimed to be at the origin of RTF in magnetically doped wide-gap oxides. This assumes that the magnetic interaction is mediated by large hydrogenic orbitals associated to intrinsic defects and predicts ferromagnetism below the donor percolation threshold, i.e., in absence of free carriers. It is then attractive since it justifies ferromagnetism deep into the insulating regime. Although the mean field T_C obtained with realistic parameters for $Zn_{1-x}Co_xO$ is extremely small ($\sim$10 K),[40] the model is frequently used to explain the experimental results.

We critically assess the DIBE model by performing Monte Carlo simulations, where the local spins $\vec{S}_k$ are treated as classical variables coupled to quantum electrons following the scheme proposed in Ref. 41. The Hamiltonian for the system is[42]

$$H = \sum_{ij} t_{ij} c_{i\sigma}^{\dagger} c_{j\sigma} + \sum_{jk} J_{kj} \vec{S}_k \cdot \left(c_{j\alpha}^{\dagger} \frac{1}{2} \vec{\sigma}_{\alpha\beta} c_{j\beta} \right), \qquad (1)$$

where $c_{i\sigma}$ ($c_{i\sigma}^{\dagger}$) is the annihilation (creation) operator for an electron at the donor site i with spin σ, k labels the cation positions of the Co ions, and $\vec{\sigma}$ is a vector of Pauli matrices. The hopping integral is a function of the separation $r_{ij}=|\vec{R}_i - \vec{R}_j|$ between two donor sites $t_{ij}=2(1+\frac{r_{ij}}{a_B})e^{-r_{ij}/r_H}$ Ry (Ry is the binding energy of the donor) and $J_{kj}=J_{\text{eff}}e^{-2|\vec{R}_k-\vec{R}_j|/r_H}$. Note that this model is similar to that used to describe (Ga,Mn)As,[41] although now the sites providing the magnetic moment are separated from those providing the donor carriers. The effective exchange coupling is $J_{\text{eff}}=J_{sd}(\frac{r_d}{r_H})^3$, where the standard *s-d* exchange J_{sd} ($\sim$1.5 eV from the red shift of the band gap with cobalt doping[40,43]) is rescaled by the ratio between the radius of the Co d shell r_d with that of the hydrogenic impurities r_H. An estimate of J_{eff} for ZnO gives us a value of 63 meV.[40] Since the mean field T_C obtained with these parameters is rather small we further rescale J_{eff} by a factor α and we investigate which value of α is needed for RTF.

Our results for a Co and donor concentrations, respectively, of 10% and 1% are presented in Fig. 1. It appears clearly that RTF is achieved only for $\alpha \geq 100$, while T_C is only a few Kelvin for $\alpha=1$. Interestingly though the magnetization curve (displayed in the inset for $\alpha=150$) has a concave upwards shape with long tails and the susceptibility χ clearly peaks at T_C. Since the uncertainty over J_{eff} is definitely smaller than a factor 100 we conclude that the DIBE model cannot account for the RTF in $Zn_{1-x}Co_xO$.

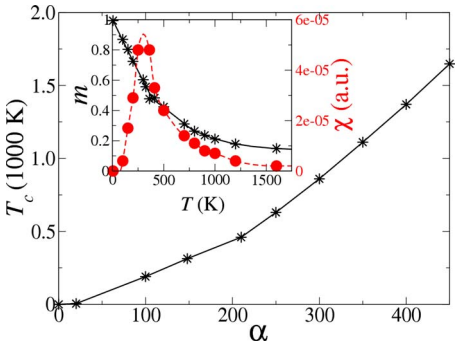

FIG. 1. (Color online) Critical temperature T_c as a function of the scaling parameter α as obtained with Monte Carlo simulations for the donor impurity band exchange model. In the inset we show the reduced magnetization $m=M/M_S$ and the magnetic susceptibility χ as a function of temperature for $\alpha=150$.

III. DENSITY-FUNCTIONAL THEORY APPROACH AND COMPUTATIONAL DETAILS

In the absence of any simple scheme for ferromagnetism we turn to atomistic density-functional theory (DFT) calculations. To investigate the (Zn,O)Co system, we adopt the pseudopotential based supercell approach which is by far the most widely used approach to model doped semiconductor systems, although some studies using accurate all electron methods but smaller supercells can also be found in the literature.[44] The choice of exchange and correlation (XC) potential is also crucial and it is widely acknowledged in the more recent literature that standard functionals such as local spin density approximation/generalized gradient approximation (LSDA/GGA) are in general not adequate to describe (Zn,Co)O and that improved XC functionals are necessary. Some of the well-known shortcomings of LSDA/GGA in describing (Zn,Co)O include the underestimation of the ZnO band gap, the underestimation of the binding energy of the Zn-3*d* states, and the overdelocalization and underbinding of the Co-*d* shell resulting in their incorrect positioning with respect to the Fermi level E_F. Similar failures only have a minor impact in the case of other transition-metal doped semiconductors such as GaAs:Mn,[45,46] but they become a serious drawback for the oxides where the Co-*d* density of states (DOS) has important contributions in the ZnO band gap. Hence beyond-LDA approaches such as LSDA $+U$/GGA$+U$,[44,47,48] hybrid DFT,[49] and empirical nonlocal external potentials (NLEP)[50] have been employed in recent times to investigate the magnetism in transition-metal ion doped ZnO. Chanier *et al.*[44] investigated the exchange couplings between substitutional Co and Mn ions in ZnO using accurate all electron based LSDA$+U$. Gopal and Spaldin[47] applied the LSDA$+U$ approach to study the magnetic interactions in ZnO for a range of transition-metal dopants and impurities. In the work of Patterson,[49] the B3LYP hybrid-

DFT functional is used to study the magnetism in (Zn,Co)O including the role of various intrinsic defects. More recently, Lany *et al.*[50] used the NLEP approach to study the effect of electron doping on the magnetic interactions between Co ions in (Zn,Co)O. In this work, we adopt an approximate self-interaction correction (ASIC) scheme,[51,52] which is free of the problems associated with LSDA/GGA and also produces exchange parameters for transition-metal monoxides superior to those obtained with LDA/GGA.[53] Furthermore, the spectra of the oxide phases of Co, such as CoO and Co_3O_4 are reproduced correctly in ASIC.[54]

It is worth noting that while most beyond-LDA methods generally improve upon the LSDA/GGA description of (Zn,Co)O, certain differences do exist in the way the methods treat various parts of the (Zn,O)Co spectrum. For example, in the commonly used LSDA+U/GGA+U approach,[44,47,48] only the d states of the dopant transition-metal ions are often corrected while the spectrum of the underlying ZnO host is left uncorrected. Thus the band gap of ZnO is still underestimated in LSDA+U and results that depend upon the position of the ZnO conduction band must be interpreted carefully.[50] Approaches such as hybrid-DFT, NLEP, and ASIC overcome this limitation by correcting both the host semiconductor states as well as the dopant transition-metal ion derived states. Still, some quantitative differences exist between the methods especially with regards to the exact location of the empty Co-t_2 states above the ZnO conduction band.

The ASIC method has been implemented numerically in the localized basis set code SIESTA.[55] In this work, the ASIC scaling parameter α was set to 1/2, which is the value appropriate for describing the electronic structure of mid- to wide-gap semiconductors.[52] In all the simulations we have considered unit cells ranging from 128 to 256 atoms. The basis set used was as follows: Zn: DZ-s, DZ-p, SZ-d, O: DZ-s, DZ-p, SZ-d, Co: DZ-s, DZP-p, DZ-d (SZ=single zeta, DZ=double zeta, DZP=double zeta polarized[55]). The grid cutoff (equivalent to plane-wave cutoff) was 650 Ry and we have considered 18 k points in the full Brillouin zone for the 128 atom cell and appropriate scaling for other cells. Standard conjugate gradient geometrical relaxation was performed until the forces were smaller than 0.04 eV/Å.

IV. RESULTS

A. Co^{2+} in ZnO: Short-range magnetic interaction

In Fig. 2 we present the DOS of a Co impurity (at the Zn site) in a 128 atom ZnO supercell (x=0.0156) calculated with both LDA and ASIC. Although they both predict a 2+ valence, the position of the Co d levels is remarkably different in the two cases. LDA places the occupied minority e states just below E_F at the edge of the ZnO conduction-band minimum (CBM). ASIC shifts these by about 2 eV down to the valence-band top (VBT) in agreement with recent calculations.[56] In addition the ZnO band gap opens and the Zn d DOS is also downshifted. This gives us a picture where there is no Co-d contribution to the DOS around E_F, with the first unoccupied minority states (t_2) placed at about 1 eV above the CBM. It is worth noting that the position of this t_2 state is reported to be ~0.5 eV, ~2.0 eV above the CBM in NLEP (Ref. 50) and hybrid-DFT (Ref. 49) calculations, respectively. Thus the ASIC value is intermediate to the two although much closer to the NLEP value. The ASIC calculated DOS for the occupied states in (Zn,Co)O is in excellent agreement with ultraviolet photoemission (UPS), which places the Co-d DOS at a binding energy of about 3 eV with a satellite peak at 7 eV and a rather diffuse tail[13] [see Fig. 3(d)]. This electronic structure is incompatible with a carrier

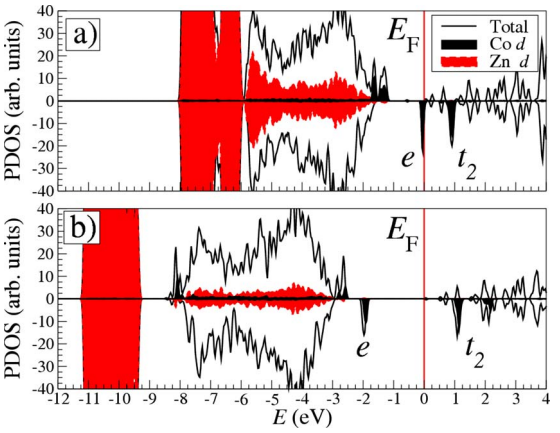

FIG. 2. (Color online) Density of states of $Zn_{1-x}Co_xO$ as calculated from density-functional theory. The simulation cell is a 128 ZnO supercell in which one Zn atom is replaced by Co (x =0.0156). Panels (a) and (b) show LDA and ASIC results, respectively.

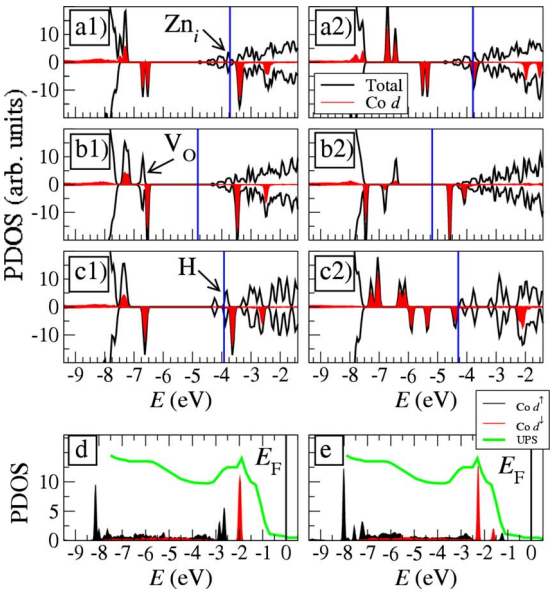

FIG. 3. (Color online) Density of states for a ZnO 128 atom supercell with one Co^{2+} and one additional defect: (a) Zn_i, (b) V_O, and (c) H. The left panels are for Co^{2+} and the defect well separated in the cell, while the right panels are for the NN position. The arrows indicate the relevant defect position. In (d) and (e) we present the Co 3d density of states as compared with UPS data from Ref. 13. (d) Co^{2+} substitutional at the Zn site, (e) $Co^{2+}-V_O$ complex. The UPS signal has been aligned to the calculated DOS in order to have the first peak at the minority Co e states.

TABLE I. (Color online) Calculated magnetic energy E_M for various magnetic centers and different dopants configuration. C1 and C2 are the two magnetic centers included in the simulation cell and their relative concentration (concentration of each center), D is the dopant with its concentration d_{C1-C2} in the distance between the two centers expressed both in Å and in NN shells. For some of the NN complexes we present the geometrical configuration (after relaxation in the pictures below).

C1 (x)	C2 (x)	D (y)	d_{C1-C2} (Å)	d_{C1-C2} (NN)	Position D	E_M (meV)	Fig.
Co (0.015)	Co (0.015)	–	3.19	1	–	−38	1
Co (0.015)	Co (0.015)	–	3.11	1	–	62	2
Co (0.015)	Co (0.015)	–	4.54	2	–	−1	-
Co (0.010)	Co (0.010)	Zn_i (0.010)	8.01	3	Far	−1	-
Co (0.010)	Co (0.010)	Zn_i^+ (0.010)	8.01	3	Far	1	-
Co (0.010)	Co (0.010)	H (0.010)	8.01	3	Far	0	-
Co (0.010)	Co (0.010)	V_O (0.010)	8.01	3	Far	−1	-
Co (0.015)	Co (0.015)	Zn_i (0.015)	3.180	1	Near	629	3
Co (0.015)	Co (0.015)	Zn_i (0.015)	2.551	1	Near	3	4
Co (0.015)	Co (0.015)	Zn_i (0.015)	2.914	1	Near	512	5
Co (0.015)	Co (0.015)	Zn_i (0.015)	2.557	1	Near	731	3
Co (0.015)	Co (0.015)	V_O (0.010)	2.585	1	Near	10	6
Co (0.015)	Co (0.015)	V_O (0.010)	2.795	1	Near	−103	-
Co (0.015)	Co (0.015)	H (0.010)	3.829	1	Near	12	7
Co (0.015)	Co (0.015)	H (0.010)	2.713	1	Near	296	8
CoV (0.015)	CoV (0.015)	–	5.55	2	–	−6	-
CoV (0.015)	CoV (0.015)	H (0.010)	2.30	1	Far	423	-
CoV (0.015)	CoV (0.015)	H (0.010)	2.27	1	Far	614	-
CoV (0.015)	CoV (0.015)	H (0.010)	5.55	2	Far	84	-
CoV (0.015)	CoV (0.015)	H (0.010)	4.51	2	Far	9	-
CoV (0.015)	CoV (0.015)	H (0.010)	6.94	3	Far	20	-

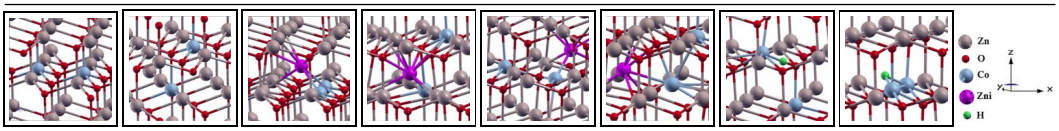

mediated picture of ferromagnetism. In fact, E_F should be moved by at least 1 eV in order to affect the Co valence and therefore to promote the charge transfer necessary for strong exchange coupling;[40] a task hardly achievable.

We test this conjecture by calculating the magnetic coupling between two Co^{2+} at various distances $d_{Co\text{-}Co}$. In Table I we show the magnetic coupling energy E_M ($E_M>0$ indicates ferromagnetic coupling), obtained as the total-energy difference between the ferromagnetic (FM) and antiferromagnetic (AFM) configurations of a selection of supercells containing two Co^{2+} and one intrinsic defect far from both the Co^{2+}. Clearly the exchange interaction between two Co^{2+} is strong only at NN position, i.e., when the superexchange interaction is effective. In this case the interaction is AFM in the a-b plane ($d_{Co\text{-}Co}$=3.19 Å) and FM along the c axis ($d_{Co\text{-}Co}$=3.11 Å). We note that in contrast to ASIC, LSDA $+U$ calculations find both the in and out-of-plane interactions also to be AFM.[44,47] Significantly, E_M drops to almost zero already at second NN, regardless of the presence of additional intrinsic defects. In particular we show data for third NN (the data for second NN are similar) in presence of either Zn_i, H, or V_O from which one has to conclude that RTF is not achievable by simply defect doping.

Figure 3 offers an insight on why Zn_i and V_O are unable to mediate RTF. We present the DOS of a 128 atom supercell containing one Co^{2+} and one intrinsic defect (V_O, Zn_i, and H), and compare the case where the Co^{2+} and the defect are well separated in the cell with that in which they are at NN position. In the case of distant defects the DOS is essentially a superposition of that of Co^{2+} and the defect. Both Zn_i and H posses a filled hydrogenic level above the CBM and rather close to the Co d-t_2 minority levels. In contrast V_O displays a doubly occupied impurity level 1 eV above the VBT, almost at the same position of the minority Co-d e levels. Most importantly there is no evidence of interaction between Co^{2+} and the defect levels (the magnetic moment calculated from the Mulliken population is $\sim$2.6 μ_B/Co for all three cases, similarly to the case of Co^{2+} only). This means that, despite the energy proximity of the defect levels to those of the Co 3d shell, the overlap of the hydrogenic wave function at the Co site is only minimal. For this reason we conclude that

the DIBE model as formulated cannot be sustained by the electronic structure of Co^{2+} in ZnO.

The right panels of Fig. 3 for NN defects give a different picture. In the case of both H and Zn_i there is a substantial charge transfer from the defects to the Co^{2+} resulting in a partial occupation of the minority t_2 levels and a reduction of the magnetic moment (1.95 μ_B/Co and 2.05 μ_B/Co, respectively, for Zn_i and H). On-site repulsion moves upwards in energy all the Co $3d$ manifold and now the majority t_2 levels occupy the ZnO band gap. In contrast, for V_O no such charge transfer occurs from the defect to the Co-d shell. In fact, the Mulliken population on the Co-d shell is found to decrease slightly by about 0.01 electrons indicating a slight broadening of the d states. More significantly, in the absence of an O ion next to the Co, the crystal field experienced by the Co ion is smaller which lowers the energy of the Co-$3d$ manifold. Furthermore, the doubly occupied V_O level spin splits by about 0.5 eV in the opposite direction to that of Co. Such a feature suggests that the exchange interaction between NN Co ions, when mediated by a defect, can be extremely large. This is indeed the case as demonstrated in Table I where E_M for various Co-Co-defect complexes is presented. Such complexes effectively behave as small metallic clusters and it is of no surprise that the exchange energy increases quite dramatically for $d_{Co\text{-}Co}$ around and below 2.5 Å, which is the NN distance in metallic Co.

Is this sufficient for RTF in the diluted phase? Unfortunately not. These interactions, although strong, are still short range and therefore produce RTF only for x around the percolation limit. Moreover, the strong FM interactions require a ratio between Co and the relevant donor of 2:1, which at percolation means typical defect concentrations of around 10%. These are impossible to achieve for any of the defects investigated even under the most favorable conditions. Finally those complex structures, if abundant, should appear spectroscopically with a substantial increase of the Co-d DOS in the ZnO band gap.

B. Magnetism of the Co^{2+}-V_O pairs impurity band

Since Co^{2+} alone cannot be responsible for RTF at low dilution we have searched for other possible magnetic centers and found that Co^{2+}-V_O pairs (CoV) overcome the limitations mentioned above, in agreement with recent experimental suggestions.[35–37] In this section we demonstrate that CoV (1) are spectroscopically compatible with UPS data, (2) are abundant, i.e., they have a low formation energy, and (3) couple ferromagnetically over long range if donors are present.

In Figs. 3(d) and 3(e) we present the DOS associated to the Co-d shell for both Co^{2+} and CoV, as compared with UPS from Ref. 13. Clearly both Co^{2+} and CoV are compatible with UPS; in particular they both show a finite DOS at about −8 eV from E_F. This feature is absent in the DOS of both the Co-Zn_i and Co-H complexes, which instead present substantial contributions in the ZnO gap and therefore are incompatible with the spectroscopy. Moreover CoV is the only complex among the ones studied which maintains Co in the 2+ valence state.

Next we have to establish whether V_O are likely to be abundant and sit preferentially close to Co^{2+} ions. The formation energy $E^f(V_O^q)$ for an oxygen vacancy (V_O) in ZnO in the charging state q has been calculated using a supercell approach well documented in the literature.[30,31] $E^f(V_O^q)$ can be expressed as

$$E^f(V_O^q) = E_{tot}(V_O^q) - E_{tot}(\mathrm{ZnO}) + \mu_O + q(E_F - E_v), \quad (2)$$

where $E_{tot}(V_O^q)$ is the total energy of a supercell containing the V_O in the charging state q, $E_{tot}(\mathrm{ZnO})$ is the total energy of the perfect ZnO crystal, μ_O is the oxygen chemical potential, E_F is the Fermi level, and E_v is the valence-band top. All the quantities entering in the Eq. (2) are calculated in terms of total-energy differences, including the valence-band top. This latter is computed as

$$\lim_{q\to 0} \frac{E_{tot}(\mathrm{ZnO}) - E_{tot}(\mathrm{ZnO} - q)}{q}, \quad (3)$$

where $E_{tot}(\mathrm{ZnO}-q)$ is the total energy of a perfect ZnO crystal where q electrons have been removed.[57] In all the calculations we consider 128 atoms supercells with identical convergence parameters (basis, k points, etc) as those used in rest of the paper.

At variance with both Refs. 30 and 31 there is no need to correct the native ZnO band gap, which is properly described by ASIC. To prove this point the band structure of a 128 ZnO supercell including one V_O in different charging states is presented in Fig. 4. Note that the band gap is about 3.5 eV with the single particle a_1 level associated to the neutral O vacancies placed at around 0.75 eV from the valence-band top.

The formation energy as a function of the position of the Fermi level for Zn-rich growth conditions is presented next in Fig. 5. Our results, in agreement with both Refs. 30 and 31 confirm that V_O is a "negative U" center, with the $E(2+|+)$ transition state placed at an higher energy than $E(+|0)$. Furthermore from the figure it is easy to note that the $E(2+|0)$ transition state is only about 1 eV above the valence-band top. This results in a formation energy for V_O in n-doped ZnO (E_F close to the conduction-band minimum) of only 0.65 eV, confirming the results of Ref. 30. Such low formation energies for V_O have also been reported in recent hybrid-DFT calculations[49,58] and demonstrate that V_O are certainly abundant in ZnO.

Our calculated V_O formation energy suggests that the V_O concentration in ZnO can be as large as 1% at equilibrium. Since Co does not introduce doping its presence will not change considerably the V_O formation energy. We have then left only to establish whether the V_O sits preferentially close to a Co site. By using a 128 atom supercell we calculate a reduction in total energy of about 340 meV for Co and V_O moving from third to first NN (pairing energy). This is quite a large gain suggesting that most of the V_O are indeed likely to be close to Co ions. The large pairing energy also means that the relative concentration of CoV (x^{CoV}) with respect to that of Co^{2+} (x^{Co}) will increase upon oxygen absorbing processing. This is the case for both annealing in an oxygen poor atmospheres and long exposure to Zn and Ti vapors.[29] In the first case one expects V_O migration to the Co sites,

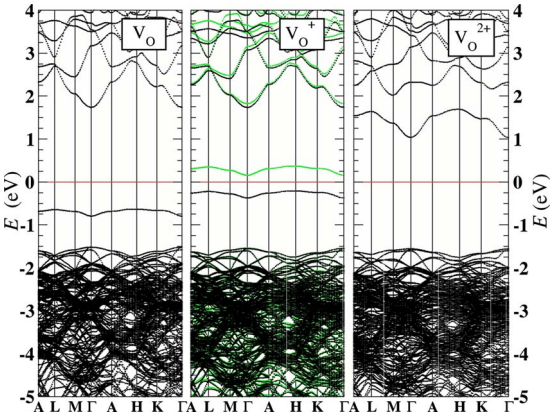

FIG. 4. (Color online) Band structure of a 128 ZnO supercell including one V_O in different charging states. In the case of V_O^+ the band structure is spin polarized and the dark and lighter shaded lines represent majority and minority spin bands, respectively.

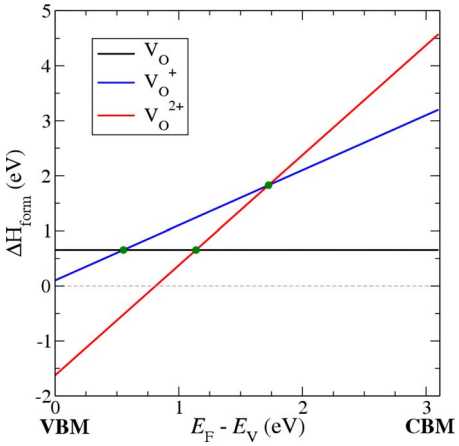

FIG. 5. (Color online) Formation energy for V_O as a function of the position of the Fermi level. Note that V_O is a "negative U" center, with the $E(2+|+)$ transition state placed at a higher energy than $E(+|0)$.

while in the second a preferential V_O formation close to Co. Finally, we found that the pairing energy between two Co^{2+} is also large (~210 meV), while we did not find any substantial pairing interaction among the CoV in any charging configuration. We then expect an inhomogeneous distribution of the Co^{2+}, which in turn would lead to an inhomogeneous distribution of CoV and the formation of both high and low-concentration regions.

Finally, we have to establish whether CoV couple at long range. Table I shows E_M for various CoV combinations. Similarly to the case of Co^{2+} also the magnetic coupling between two charge neutral CoVs is remarkably weak already at second NN (−6 meV). However, when an additional electron donor is present, the situation changes dramatically with second and third NN magnetic couplings reaching up, respectively, to $E_M \sim 80$ meV and $E_M \sim 20$ meV. Note that we cannot exclude an even longer interaction range, which however is hardly accessible in our simulations since the size of the supercells becomes prohibitively large.

Why does CoV sustain long-range coupling while Co^{2+} does not? The cartoon of Fig. 6(a) shows the electronic structure of Co^{2+}, V_O, and CoV. The main feature is that the Co^{2+} empty t_2 minority state broadens in CoV and forms a t_2-V_O hybrid level right at the CBM. This extends in space over the first shell of Zn ions and an impurity band forms already at tiny concentrations. Such a band can be easily n doped. Thus, while for Co^{2+} the only exchange mechanisms available either involve virtual transitions or weak s-d (Ref. 59) exchange interaction with hydrogenic orbitals, for CoV strong carrier-mediated magnetic interaction is possible. In Fig. 6(b) we show E_M for two CoV in a 128 atom unit cell as a function of the electron doping. This is introduced by either moving E_F in our simulations or by explicitly introducing an H ion in the supercell. Clearly E_M depends strongly on the occupation of the impurity band, with a maximum at half filling ($n=6.7\times10^{20}$ cm^{-3}) and vanishing for $n=0$ (empty band). Note that as n is increased, beyond a certain point ($n\sim8\times10^{20}$ cm^{-1}), E_M is seen to flatten out. This is because, as the occupation of the minority Co-t_2 states increases, the on-site coulomb repulsion causes the energy of the Co-3d manifold to increase. This causes the minority t_2 states, initially located just below the CBM, to merge with the conduction-band (CB) states. Beyond this point, extra charge carries prefer to occupy CB states and the occupation of the Co-t_2 states remains almost constant as they are pinned just above the Fermi level. We therefore expect the valence state of Co ions in Co-V complexes even in the presence of additional charge carriers to be $Co^{(2-\delta)+}$ where $0<\delta<1$.

C. Two-center model and phase diagram

Thus DFT offers us a mechanism for the ferromagnetism in (Zn,Co)O based on two magnetic centers: Co^{2+} is responsible only for short-range coupling, while CoV can instead sustain long-range interaction via a fractionally filled impurity band. Can this alone produce RTF? Percolation theory[60] sets a strict condition for a magnetic ground state of diluted systems: the concentration of magnetic impurity should exceed the percolation threshold x_c. This depends on the range of the interaction and for the fcc lattice we find 19.8%, 13.7%, and 6.2% for interaction extending, respectively, to first, second, and third NN.[61] Therefore our two-center model already produces long-range ferromagnetism at $x^{CoV}>x_c \sim 6\%$. However, we do not need such a large x for observing hysteresis in the M-H curve at room temperature (i.e., for explaining the various experimental claims). This can be achieved below x_c since one just needs a number of percolating clusters large enough to be superparamagnetically blocked. Note that "clusters" here mean regions where x is locally larger than x_c. The presence of CoV pushes this limit far below the 20% needed by Co^{2+} and by the recently proposed model where the magnetism originates from uncompensated spins at the surface of antiferromagnetic clusters.[62]

The size of those clusters can be estimated by considering coherent rotation of the magnetization over an anisotropy barrier DN_BS^2 (D is the zero-field splitting, N_B the number of magnetic ions magnetically blocked, and S the Co spin). By

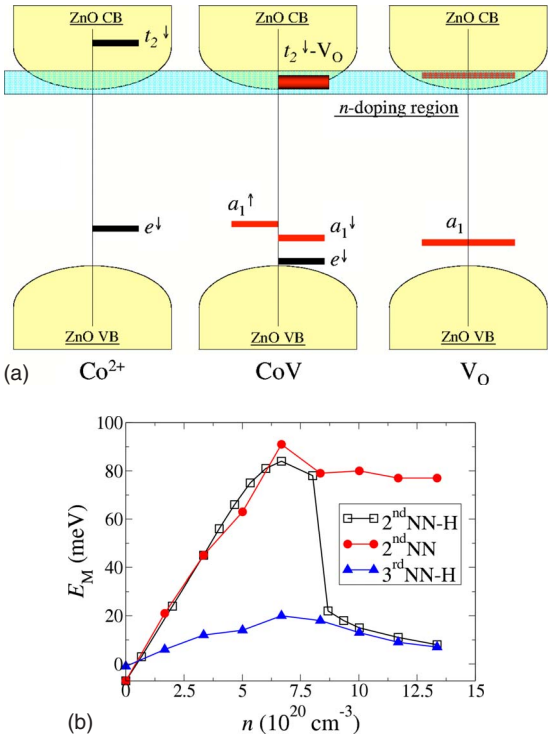

FIG. 6. (Color online) CoV impurity band. (a) Level diagram for Co^{2+}, V_O, and CoV. (b) E_M for two second NN CoV as a function of the donor impurity band electron density. The electron density 6.7×10^{20} cm^{-3} corresponds to one electron every two CoV.

taking $D=2.76$ cm^{-1} from electron paramagnetic resonance (EPR) measurements[18] we obtain the estimate $N_B \sim 800$ for a blocking temperature $T_B=300$ K. This however is rather conservative. In granular magnets random dipolar interaction,[63] random magnetic anisotropy,[64] or spinodal decomposition[65] can push T_B to values considerably larger than those predicted for single-particle coherent rotation (up to a factor 5). Thus we estimate N_B in the range of 250 magnetic ions. Therefore, an observation of a hysteresis requires the existence of regions where 250 CoV ions interacting at third NN exist at concentrations larger than $\sim 6\%$. Indeed this is a rather modest requirement.

In Fig. 7(a) we present typical cluster distributions $P(N)$ as a function of the cluster size N for various concentrations of Co^{2+} and CoV. These have been obtained by filling randomly a wurtzite lattice comprising 10^6 sites. As expected $P(N)$ moves from small to large clusters as x^{CoV} is increased with respect to x^{Co}. In particular one notes that already for $x^{CoV}=2\%$ large clusters appear in the distribution, which becomes bimodal at $x^{CoV}>6\%$, i.e., above x_c. We emphasize that these $P(N)$ have been obtained from a completely random distribution, i.e., neglecting the tendency to clustering suggested by the pairing energy.

Finally, we investigate the thermodynamical properties of our two-center model by performing Monte Carlo simulations for a Heisenberg energy ($|\mathbf{S}_i|=1$),

$$\mathcal{H}_{\text{eff}} = \sum_{\langle i,j \rangle}^{\text{Co,CoV}} J_{ij}\mathbf{S}_i \cdot \mathbf{S}_j . + \sum_{i}^{\text{Co,CoV}} D(\mathbf{S}_i \cdot \hat{n})^2. \quad (4)$$

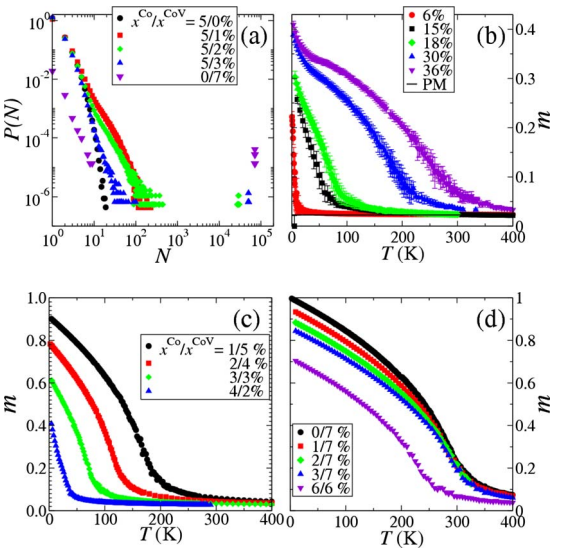

FIG. 7. (Color online) Monte Carlo simulations for the two-center model: (a) cluster distribution $P(N)$ as a function of the number N of magnetic ions in the cluster for different x^{Co} and x^{CoV} (x^{Co}/x^{CoV}); (b) magnetization curves $m(T)$ at different Co concentration for $x^{Co}/x^{CoV}=5$; (c) $m(T)$ for a total Co concentration of 6% and different x^{Co}/x^{CoV}; (d) $m(T)$ for x^{CoV} above percolation (7%) and various x^{Co} (x^{Co}/x^{CoV}).

The exchange parameters are chosen to mimic the short and long-range exchanges between Co^{2+} and CoV, respectively. At NN J_{ij} is AFM for Co^{2+} pairs (15 meV) and FM for CoV pairs (50 meV) and between Co^{2+} and CoV (50 meV). Moreover it extends to second (15 meV) and third NNs (5 meV) for CoV pairs. The last term accounts for an hard-axis (easy-plane) anisotropy ($|\hat{n}|=1$).[18] Note that we implicitly assume doping in the CoV impurity band and neglect the NN FM component of the exchange between Co^{2+} pairs. Given the uncertainty over the precise microscopic configuration and the relative abundance of the various complexes (Table I) our numerical values are only representative and certainly conservative. However, even with this choice $T_c=250$ K above percolation ($x^{CoV}=7\%$) suggesting that RTF is indeed possible.

Monte Carlo simulations were performed with the Metropolis algorithm as implemented in a home-made package. Typical simulation cells for the two-center Heisenberg model contain between 1600 and 5000 magnetic ions and we always use periodic boundary conditions. The systems are equilibrated until an initially AFM and FM replicas have converged to the same value (typically 10 000 steps) and then the Monte Carlo measurements are taken by sampling 60 000 new steps. Disorder averages have taken over 32 different samples at each concentration. The Curie temperature T_C for the two-center model (Co^{2+} and CoV) is calculated from the specific heat C of a diluted system. In Fig. 8 we present results for $x^{CoV}=7\%$, i.e., for a concentration above percolation (third NN percolation of the fcc lattice). Clearly the critical temperature T_c is around 250 K.

In Fig. 7(b) we present the reduced magnetization $m=M/M_s$ as a function of T for different Co concentrations,

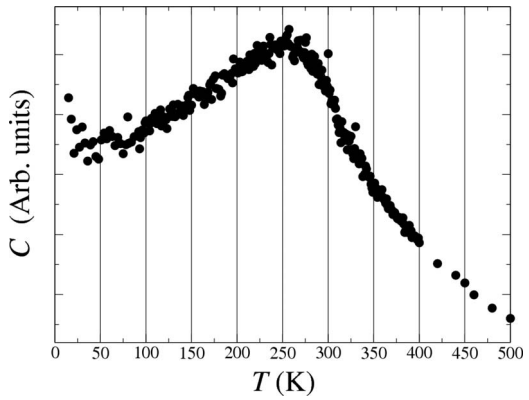

FIG. 8. Specific heat C as a function of temperature T for the two-center model at $x^{CoV}=7\%$ and $x^{Co}=0\%$. The peak in $C(T)$ denotes the position of the Curie temperature T_C. Each point in the graph is an average of over 32 disorder configurations.

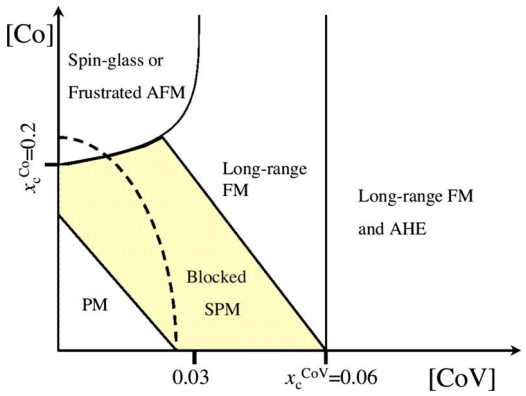

FIG. 9. (Color online) Proposed phase diagram for (Zn,Co)O as a function of the relative concentrations of Co and CoV. The yellow area is the blocked superparamagnetic (SPM) region, where both magnetic moment and hysteresis can be detected. The dashed line at small x delimits the region where most of the experiments are conducted. Finally the FM region is partition into two regions depending on whether or not anomalous Hall effect can be detected.

while keeping $x^{Co}/x^{CoV}=5$. The magnetization curves show a transition from a concave upwards shape at low concentrations to a convex one for high. As the concentration increases one encounters the two percolation thresholds, respectively, for CoV and for Co. This produces the change in shape, which however is complete only above 20%, i.e., when the Co^{2+}'s start to percolate. Interestingly m never reaches 1 because of the strong NN AFM interaction among Co.

We also investigate the interplay between Co^{2+} and CoV. In Fig. 7(c) $m(T)$ is calculated by keeping the total Co concentration to 6% and by varying the ratio between x^{Co} and x^{CoV}, while in Fig. 7(d) we keep $x^{CoV}=7\%$ (above percolation) and change x^{Co}. In both pictures x^{Co} is well below the percolation threshold for NN and the high-temperature region of $m(T)$ is almost entirely dominated by x^{CoV}. For instance one may note that for $x^{CoV}=5\%$ $m(T)$ approaches zero roughly at the same T regardless of whether x^{Co} is 1% [Fig. 7(c)] or 25% [Fig. 7(b) for a total concentration of 30%]. In contrast the amount of Co^{2+} affects the low-temperature region, where the strong AFM interaction can drastically alter the total magnetic moment. For instance $m(0)$ drops from 1 to about 0.8 if x^{Co} is increased from 1% to 3%, by keeping $x^{CoV}=7\%$.

We are now in a position to propose a phase diagram for (Zn,Co)O based on the relative concentration of Co^{2+} and CoV (Fig. 9). The most important feature is the presence of what we called a blocked superparamagnetic phase.

This is below x_c^{CoV} and x_c^{Co}, but nevertheless allows one the detection of both a net magnetic moment and hysteresis at room temperature. For larger x a long-range FM ground state emerges, which however is limited by the short-range AFM interaction of the Co ions. Therefore we predict either a frustrated antiferromagnet or a spin glass for $x^{Co}>x_c^{Co}$ and $x^{CoV}\ll x^{Co}$. We emphasize that bulk measurements (hysteresis or magnetization) can hardly distinguish between the FM and the blocked superparamagnetic phase, and more local probes are needed. In particular further insights would be provided by a thorough analysis of small-angle neutron-scattering data similar to the case of disordered ferromagnets.[64] Alternatives may be muon rotation, high-resolution EPR, and energy-dispersive x-ray spectroscopy.

Finally we partition the long-range FM region into two regions separated by the CoV percolation threshold x_c^{CoV}. For $x^{CoV}>x_c^{CoV}$ percolation among CoV is achieved and one expects measurable conductivity from the impurity band. Since the exchange is strong an anomalous Hall effect (AHE) should be detected. This is not expected for ferromagnetism below x_c^{CoV} since the conductivity is then dominated by band conductivity which is weakly affected by Co^{2+}, given the small exchange. Note that this phase diagram says little about the overall conductivity of (Zn,Co)O, which in turn can be determined by electrons in the conduction band. Moreover, the precise location of the phase boundaries depends on details such as the concentration of electron donors. In the extreme case of fully compensated samples the blocked superparamagnetic phase may even disappear entirely.

V. CONCLUSION

In conclusion, by using a combination of DFT and Monte Carlo simulations, we have demonstrated that the observed RTF in (Zn,Co)O can be attributed to blocked superparamagnetism. This develops at concentrations below those required by long-range ferromagnetism. However, even this model requires a second magnetic dopant in addition to Co^{2+} substituting Zn, capable of mediating magnetic interaction beyond nearest neighbors. We have identified the Co-V_O pair as the most likely candidate and demonstrated that such center can indeed promote long-range coupling, if additional n doping is present. These findings draw a new roadmap for designing diluted magnetic oxides, where the engineering of intrinsic defects play the leading role. For instance paramagnetic samples can be turned ferromagnetic by prolonged exposure to Ti vapors, which produce high concentrations of V_O.[29]

ACKNOWLEDGMENTS

This work is sponsored by Science Foundation of Ireland under Grants No. SFI02/IN1/I175 and No. 05/IN1/I853. Computational resources have been provided by the HEA IITAC project managed by the Trinity Center for High Performance Computing and by ICHEC.

[1] V. E. Wood and A. E. Austin, *Magnetoelectric Interaction Phenomena in Crystal* (Gordon and Breach, London, 1975).
[2] Special issue on Transparent Conducting Oxides, edited by D. S. Ginley and C. Bright [MRS Bull. **25** (2000)].
[3] D. D. Awschalom, D. Loss, and N. Samarth, *Semiconductor Spintronics and Quantum Computing* (Springer, Heidelberg, 2002).
[4] M. H. Huang, S. Mao, H. Feick, H. Yan, Y. Wu, H. Kind, E. Weber, R. Russo, and P. Yang, Science **292**, 1897 (2001).
[5] M. Kroutvar, Y. Ducommun, D. Heiss, M. Bichler, D. Schuh, G. Abstreiter, and J. J. Finley, Nature (London) **432**, 81 (2004).
[6] A. H. MacDonald, P. Schiffer, and N. Samarth, Nat. Mater. **4**, 195 (2005).
[7] K. Ueda, H. Tabata, and T. Kawai, Appl. Phys. Lett. **79**, 988 (2001).
[8] K. Rode, A. Anane, R. Mattana, J.-P. Contour, O. Durand, and R. LeBourgeois, J. Appl. Phys. **93**, 7676 (2003).
[9] W. Prellier, A. Fouchet, B. Mercey, Ch. Simon, and B. Raveau, Appl. Phys. Lett. **82**, 3490 (2003).
[10] M. Venkatesan, C. B. Fitzgerald, J. G. Lunney, and J. M. D. Coey, Phys. Rev. Lett. **93**, 177206 (2004).
[11] H.-J. Lee, S.-Y. Jeong, C. R. Cho, and C. H. Park, Appl. Phys. Lett. **81**, 4020 (2002).
[12] A. C. Tuan, J. D. Bryan, A. B. Pakhomov, V. Shutthanandan, S. Thevuthasan, D. E. McCready, D. Gaspar, M. H. Engelhard, J. W. Rogers, Jr., K. Krishnan, D. R. Gamelin, and S. A. Chambers, Phys. Rev. B **70**, 054424 (2004).
[13] M. Kobayashi, Y. Ishida, J. l. Hwang, T. Mizokawa, A. Fujimori, K. Mamiya, J. Okamoto, Y. Takeda, T. Okane, Y. Saitoh, Y. Muramatsu, A. Tanaka, H. Saeki, H. Tabata, and T. Kawai, Phys. Rev. B **72**, 201201(R) (2005).
[14] S. C. Wi, J. S. Kang, J. H. Kim, S. B. Cho, B. J. Kim, S. Yoon, B. J. Suh, S. W. Han, K. H. Kim, K. J. Kim, B. S. Kim, H. J. Song, H. J. Shin, J. H. Shim, and B. I. Min, Appl. Phys. Lett. **84**, 4233 (2004).
[15] Y. Z. Peng, T. Liew, T. C. Chong, W. D. Song, H. L. Li, and W. Liu, J. Appl. Phys. **98**, 114909 (2005).
[16] A. S. Risbud, N. A. Spaldin, Z. Q. Chen, S. Stemmer, and R. Seshadri, Phys. Rev. B **68**, 205202 (2003).
[17] A. Ney, K. Ollefs, S. Ye, T. Kammermeier, V. Ney, T. C. Kaspar, S. A. Chambers, F. Wilhelm, and A. Rogalev, Phys. Rev. Lett. **100**, 157201 (2008).
[18] P. Sati, R. Hayn, R. Kuzian, S. Regnier, S. Schafer, A. Stepanov, C. Morhain, C. Deparis, M. Laugt, M. Goiran, and Z. Golacki, Phys. Rev. Lett. **96**, 017203 (2006).
[19] G. L. Liu, Q. Cao, J. X. Deng, P. F. Xing, Y. F. Tian, Y. X. Chen, S. S. Yan, and L. M. Mei, Appl. Phys. Lett. **90**, 052504 (2007).
[20] L. S. Dorneles, M. Venkatesan, R. Gunning, P. Stamenov, J. Alaria, M. Rooney, J. G. Lunney, and J. M. D. Coey, J. Magn. Magn. Mater. **310**, 2087 (2007).
[21] A. Dinia, G. Schmerber, C. Mény, V. Pierron-Bohnes, and E. Beaurepaire, J. Appl. Phys. **97**, 123908 (2005).
[22] J. Cui and U. Gibson, Phys. Rev. B **74**, 045416 (2006).
[23] H. S. Hsu, J. C. A. Huang, Y. H. Huang, Y. F. Liao, M. Z. Lin, C. H. Lee, J. F. Lee, S. F. Chen, L. Y. Lai, and C. P. Liu, Appl. Phys. Lett. **88**, 242507 (2006).
[24] X. Han, G. Wang, J. Jie, X. Zhu, and J. G. Hou, Thin Solid Films **491**, 249 (2005).
[25] N. Khare, M. J. Kappers, M. Wei, M. G. Blamire and J. L. MacManus-Driscoll, Adv. Mater. (Weinheim, Ger.) **18**, 1449 (2006).
[26] H.-J. Lee, C. H. Park, S.-Y. Jeong, K.-J. Yee, C. R. Cho, M.-H. Jung, and D. J. Chadi, Appl. Phys. Lett. **88**, 062504 (2006).
[27] A. J. Behan, A. Mokhtari, H. J. Blythe, D. Score, X.-H. Xu, J. R. Neal, A. M. Fox, and G. A. Gehring, Phys. Rev. Lett. **100**, 047206 (2008).
[28] T. C. Kaspar, T. Droubay, S. M. Heald, P. Nachimuthu, C. M. Wang, V. Shutthanandan, C. A. Johnson, D. R. Gamelin, and S. A. Chambers, New J. Phys. **10**, 055010 (2008).
[29] F. A. Selim, M. H. Weber, D. Solodovnikov, and K. G. Lynn, Phys. Rev. Lett. **99**, 085502 (2007).
[30] S. Lany and A. Zunger, Phys. Rev. Lett. **98**, 045501 (2007).
[31] A. Janotti and C. G. Van de Walle, Phys. Rev. B **76**, 165202 (2007).
[32] D. A. Schwartz and D. R. Gamelin, Adv. Mater. (Weinheim, Ger.) **16**, 2115 (2004).
[33] K. R. Kittilstved, D. A. Schwartz, A. C. Tuan, S. M. Heald, S. A. Chambers, and D. R. Gamelin, Phys. Rev. Lett. **97**, 037203 (2006).
[34] A. O. Ankiewicz, J. Appl. Phys. **101**, 024324 (2007).
[35] J. S. Thakur, G. W. Auner, V. M. Naik, C. Sudakar, P. Kharel, G. Lawes, R. Suryanarayanan, and R. Naik, J. Appl. Phys. **102**, 093904 (2007).
[36] X.-C. Liu, E.-W. Shi, Z.-Z. Chen, B.-Y. Chen, T. Zhang, L.-X. Song, K.-J. Zhou, M.-Q. Cui, W.-S. Yan, Z. Xie, B. He, and S.-Q. Wei, J. Phys.: Condens. Matter **20**, 025208 (2008).
[37] X.-C. Liu, E.-W. Shi, Z.-Z. Chen, T. Zhang, B.-Y. Chen, W. Huang, X. Li, L.-Xi. Song, K.-J. Zhou, and M.-Q. Cui, Appl. Phys. Lett. **92**, 042502 (2008).
[38] T. Dietl, H. Ohno, F. Matsukura, J. Cibert, and D. Ferrand, Science **287**, 1019 (2000).
[39] J. B. Goodenough, *Magnetism and Chemical Bond* (Wiley, New York, 1963).
[40] J. M. D. Coey, M. Venkatesan, and C. B. Fitzgerald, Nat. Mater. **4**, 173 (2005).
[41] M. P. Kennett, M. Berciu, and R. N. Bhatt, Phys. Rev. B **66**, 045207 (2002).
[42] R. Hanafin and S. Sanvito, J. Magn. Magn. Mater. **316**, 218 (2007).
[43] K. J. Kim and Y. R. Park, Appl. Phys. Lett. **81**, 1420 (2002).
[44] T. Chanier, M. Sargolzaei, I. Opahle, R. Hayn, and K. Koepernik, Phys. Rev. B **73**, 134418 (2006).

[45] M. Wierzbowska, D. Sánchez-Portal, and S. Sanvito, Phys. Rev. B **70**, 235209 (2004).
[46] A. Filippetti, N. A. Spaldin, and S. Sanvito, Chem. Phys. **309**, 59 (2004).
[47] Priya Gopal and Nicola A. Spaldin, Phys. Rev. B **74**, 094418 (2006).
[48] Chang-Hong Chien, Shan Haw Chiou, G. Y. Guo, and Yeong-Der Yao, J. Magn. Magn. Mater. **282**, 275 (2004).
[49] C. H. Patterson, Phys. Rev. B **74**, 144432 (2006).
[50] Stephan Lany, Hannes Raebiger, and Alex Zunger, Phys. Rev. B **77**, 241201(R) (2008).
[51] A. Filippetti and N. A. Spaldin, Phys. Rev. B **67**, 125109 (2003).
[52] C. D. Pemmaraju, T. Archer, D. Sánchez-Portal, and S. Sanvito, Phys. Rev. B **75**, 045101 (2007).
[53] A. Akande and S. Sanvito, J. Chem. Phys. **127**, 034112 (2007).
[54] C. D. Pemmaraju and S. Sanvito (unpublished).
[55] J. M. Soler, E. Artacho, J. D. Gale, A. Garcia, J. Junquera, P. Ordejon, and D. Sanchez-Portal, J. Phys.: Condens. Matter **14**, 2745 (2002).
[56] M. Toyoda, H. Akai, K. Sato, and H. Katayama-Yoshida, Physica B (Amsterdam) **376-377**, 647 (2006).
[57] C. Persson, Y.-J. Zhao, S. Lany, and A. Zunger, Phys. Rev. B **72**, 035211 (2005).
[58] Fumiyasu Oba, Atsushi Togo, Isao Tanaka, Joachim Paier, and Georg Kresse, Phys. Rev. B **77**, 245202 (2008).
[59] B. E. Larson, K. C. Hass, H. Ehrenreich, and A. E. Carlsson, Phys. Rev. B **37**, 4137 (1988).
[60] D. Stauffer and A. Aharony, *Introduction to Percolation Theory* (Taylor & Francis, London, 1994).
[61] J. Osorio-Guillén, S. Lany, S. V. Barabash, and A. Zunger, Phys. Rev. B **75**, 184421 (2007).
[62] T. Dietl, T. Andrearczyk, A. Lipińska, M. Kiecana, M. Tay, and Y. Wu, Phys. Rev. B **76**, 155312 (2007).
[63] P. Allia, M. Coisson, P. Tiberto, F. Vinai, M. Knobel, M. A. Novak, and W. C. Nunes, Phys. Rev. B **64**, 144420 (2001).
[64] J. F. Löffler, H. B. Braun, and W. Wagner, Phys. Rev. Lett. **85**, 1990 (2000).
[65] K. Sato, T. Fukushima, and H. Katayama-Yoshida, Jpn. J. Appl. Phys., Part 2 **46**, L682 (2007).